Heliyon 10 (2024) e29496

Contents lists available at ScienceDirect

Heliyon

journal homepage: www.cell.com/heliyon

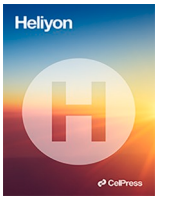

Research article

Structural, mechanical, wear and anticorrosive properties of CrSiCN coatings used for industrial woodworking applications

Iulian Pana [a], Anca Constantina Parau [a], Mihaela Dinu [a], Catalin Vitelaru [a], Diana Maria Vranceanu [b,c], Thomas Lindner [d], Alina Vladescu (Dragomir) [a,e,*]

[a] National Institute of Research and Development for Optoelectronics - INOE 2000, Department for Advanced Surface Processing and Analysis by Vacuum Technologies, 409 Atomistilor St., RO77125, Magurele, Romania
[b] Faculty of Materials and Science Engineering, University Politehnica of Bucharest, 313, Spl. Independentei, 060042 Bucharest, Romania
[c] Drugon International SRL, 2 Tractorului St., Constanta, Romania
[d] Chemnitz University of Technology, Institute of Materials Science and Engineering, Chair of Materials and Surface Engineering, D-09107 Chemnitz, Germany
[e] Research School of Chemistry & Applied Biomedical Sciences, National Research Tomsk Polytechnic University, Tomsk, 634050, Russia

ARTICLE INFO

Keywords:
CrSiCN coatings
Steel substrates
Mechanical properties
Corrosion resistance
Woodworking applications

ABSTRACT

The woodworking applications are a fast-growing field that aims to create advanced coatings with superior wear resistance, reduced friction, and robust corrosion protection. Chromium silicon carbonitride (CrSiCN) coatings have emerged as a promising solution that offers a unique combination of properties ideal for various industrial applications. The C/N ratio significantly influences the coatings' mechanical and tribological properties. By optimizing the C/N ratio, this research aims to reveal new insights for CrSiCN coatings, enhancing their application in environments that require durability, efficiency, and longevity. In this paper, the effect of the C/N ratio on the structural, mechanical, and corrosion resistance of CrSiCN coatings deposited by cathodic arc evaporation on different steel substrates was studied. The main purpose was to enhance the mechanical and anticorrosion properties of the CrSiCN coatings and to select the optimum parameters for the deposition of layers with superior properties. The results showed that the final properties can be tailored by choosing specific deposition conditions. In this case, the C/N ratio proved to be critical since coatings with higher carbon content presented enhanced corrosion resistance, being able to withstand operating conditions similar to real-life.

1. Introduction

Forests are a vital part of the planet, covering about 29 % of the Earth's surface. As a renewable resource, wood is crucial in various industries, such as residential and non-residential construction [1], furniture manufacturing [2], heating [3], or packaging [4]. Wood product manufacturing industries invest in modern tools and processing technologies to increase their output while reducing production costs [5]. Wood and wood-based product processing efficiency depend on the durability of the used tools, which leads to shorter downtime and lower maintenance costs [6]. In various manufacturing industries, wear-resistant materials have become

* Corresponding author. National Institute of Research and Development for Optoelectronics - INOE 2000, Department for Advanced Surface Processing and Analysis by Vacuum Technologies, 409 Atomistilor St., RO77125, Magurele, Romania.
E-mail address: alinava@inoe.ro (A. Vladescu (Dragomir)).

https://doi.org/10.1016/j.heliyon.2024.e29496
Received 21 December 2023; Received in revised form 22 March 2024; Accepted 9 April 2024
Available online 14 April 2024

essential in producing high-quality goods with enhanced durability [7]. These materials are designed to withstand wear, abrasion, and corrosion, ensuring that the products remain functional for an extended period. In this context, it is important to improve the mechanical and anticorrosive properties of wear-resistant materials [8,9]. Metallic alloys are generally used as substrates for hard coatings due to their excellent mechanical properties [10,11]. However, the choice of a proper metallic alloy can impact the effectiveness of the hard coating [12,13]. The use of nanocomposite coatings and advanced alloys with enhanced corrosion resistance properties represents a growing trend in wear-resistant coatings [14,15]. Surface engineering techniques, such as surface modification and surface patterning, are also explored to improve the corrosion resistance of both substrates and coatings [16]. The chromium nitride (CrN) coatings applied to carbide tools for routing of oriented strand boards (OSBs) have favourable chemical and structural characteristics and provide better wear resistance, resulting in a service life that is four times longer than that of uncoated tools [17]. Several attempts have been made to enhance the tribological performance and hardness of CrN-based coatings [18–22]. These approaches involve alloying, multilayering, or microstructure modification. Chromium carbonitride (CrCN) compounds have shown improved wear resistance and hardness, combining the mechanical properties of carbonitrides and the corrosion resistance of Cr-based coatings [23–25]. A. Gilewicz et al. demonstrated the effectiveness of multilayer CrN/CrCN coatings obtained by the cathodic arc evaporation technique in reducing wear on planer knives during the milling of beechwood [26]. The CrN/CrCN coatings exhibit good anti-wear properties, with the friction coefficient decreasing as loading increases, while the wear resistance of coatings with 1:1 and 2:1 thickness ratio is similar. The coatings significantly reduce the wear of planer knives, resulting in cutting edges with two to three times higher lifetime between regrindings. Additionally, the CrN/CrCN coatings prevent the deterioration of the surface roughness of processed wood during milling. Also, the hardness of CrN coatings can be tailored by controlling the Si and C additions [23,27,28]. After the Si addition, microstructural changes can produce fine crystallite and nanocomposite structures, improving the hardness of CrSiCN coatings. The research is distinct from previous research as its main focus is on the effect of the C/N ratio on CrSiCN coatings [29–33]. For example, while Yean-Liang Su et al. examined NbCrC49 coatings, this research offers a comprehensive examination of how different carbon and nitrogen levels have a direct impact on the properties of CrSiCN coatings. L. Constantin et al. [34] found that CrSiCN coatings demonstrated superior hardness and friction performance compared to CrN coatings, attributing this to the presence of C and Si in the film composition. Zhiwei Wu et al. [35] showed that CrSiCN coatings exhibited a nanocomposite microstructure with a maximum hardness of 19.1 GPa at a specific TMS flow rate. They also noted better friction and wear properties in tribopairs. A study by F. Cai et al. [36] found that adding Si and C to CrN coatings changed the microstructure and improved wear resistance, with the CrSiCN-2 coating having significantly lower wear rates. Qianzhi Wang et al. [32] found that quaternary CrSiCN coatings had higher resistance to radial cracks compared to ternary CrSiC coatings, regardless of the Si concentration. Therefore, this research is focused on the unresolved challenge of optimizing the C/N ratio in CrSiCN coatings to enhance both corrosion resistance and mechanical properties. This information is particularly relevant for industrial applications, such as in woodworking tools, where durable and high-performing coatings are essential for challenging operational conditions. Therefore, the findings mark a significant advancement in coating technology, comparable to other research studies [33].

The purpose of this study is to investigate the effect of different C/N ratios on the structural, mechanical, and corrosion resistance of CrSiCN coatings deposited by cathodic arc evaporation on three steel substrates (Carbon Steel C45, 16MnCr5 (1.7131), and X155CrVMo12) characterized by a different carbon content. The CrSiCN layers were investigated for elemental and phase composition, microstructure, mechanical properties, corrosion resistance, and tribological behaviour.

2. Materials and methods

2.1. Substrate alloys

Three commercially available alloy substrates with unique Fe/C elemental compositions were used as follows: carbon steel C45 (Otai Special Steel), 16MnCr5 (1.7131) (Hunan Fushun Metal Co., Ltd.), and X155CrVMo12 (SIJ Metal Ravne). The C45 steel has the lowest carbon content compared to other substrates and is suitable for strength and it toughness applications. According to producer, C45 steel round bars that have been quenched and tempered are in high demand for their remarkable strength and wear resistance, especially when compared to low-carbon mild steel. 16MnCr5 (1.7131) steel has a moderate carbon content and it is suitable for high-strength applications such as gears or cutting tools. X155CrVMo12 has the highest carbon content and it is ideal for long-run tooling applications such as cutting and molding tools, rolling dies, stamping, and within wood processing stages.

2.2. Coating deposition

The coatings were deposited using a reactive cathodic arc evaporation (CAE) unit equipped with a CrSi cathode (85 at.% Cr, 15 at. %, 99.9 % purity) supplied by Kurt Lesker (UK). The CrSi cathode diameter (Φ) was 120 mm with a corresponding thickness (δ) of 16 mm. The coatings were deposited on both polished steel substrates ($\Phi = 20$ mm, $\delta = 5$ mm, $R_a = 50$ nm) and p-type silicon <100> wafers ($\Phi = 50.8$ mm, $\delta = 0.8$ mm). Before deposition, the substrates were ultrasonically cleaned with isopropyl alcohol (CAS 67-63-0, 99.9 % purity) for 15 min in an ultrasonic bath and the deposition chamber (700 x 700 × 700 mm^3) was pumped down to a base pressure of 6×10^{-4} Pa. The substrate holder was biased at −1000 V, and the substrates were sputter etched in an Ar^+ plasma for 15 min at a pressure of 0.2 Pa. The high-purity acetylene (C_2H_2, 30, 50 or 70 sccm) and nitrogen (N_2, 70, 50 or 30 sccm) gas flow ratios were varied to increase the C/N ratio for all deposited layers. During each deposition run, the arc current on the CrSi cathode was 90 A, and the substrate holder was biased at −200 V for 40 min deposition time at a working pressure of 8×10^{-2} Pa.

In the present study, the used substrates are labeled as S1 – X155CrVMo12, S2 – 16MnCr5 (1.7131), and S3 – carbon steel C45,

while the CrSiCN coatings will be referred to as a function of deposition conditions as follows: CrSiCN C30N70, CrSiCN C50N50 and CrSiCN C70N30 for C_2H_2/N_2 reactive gas mixtures of 30/70, 50/50 and 70/30, respectively.

2.3. Morphology, microstructural and mechanical analysis

The coatings' elemental composition and surface morphology were investigated using the scanning electron microscope (SEM, TableTop 3030PLUS) with an energy-dispersive X-ray spectrometer (EDS). The X-ray diffraction (XRD) was performed using a Rigaku Miniflex II diffractometer (Rigaku, Tokyo, Japan) to determine the phase composition of the samples. The diffraction patterns were recorded from 20° to 100° 2θ range at a scan speed of 1°/minute. The coatings thickness was measured using a surface profilometer (Dektak 150) after removing the mask partially covering the Si wafers substrate during the deposition process. The substrate-layer interface was scanned using a 2.5 μm curvature radius tip over a distance of 2 mm and the height difference was then evaluated.

Friction and wear measurements under corrosive conditions (60 mL of distilled water and 0.6 g of sand) were carried out using a homemade pin on disc tribometer, the tests were performed at 22 °C room temperature and 55 % relative humidity. For this experiment, a 10 N normal load was applied over a 400 m sliding distance at 0.15 m/s speed. The pin used as a counterpart consisted of a 6 mm diameter synthetic sapphire ball. Cross-sectional profiles of the wear tracks were used to determine the worn volume (provided by the Dektak surface profilometer), and the corresponding wear rates were calculated according to Eq. (1):

$$R = V/F * d \quad (1)$$

where V = worn volume, F = normal load and d = sliding distance.

The adhesion of thin CrSiCN layers to S1–S3 substrates was evaluated using the scratch test method (performed according to the standard BS EN 1071-3: 2005), where a progressive load was applied. The force applied to the indenter increased linearly as it moved along the tested surface at a constant speed. The tests were conducted over a distance of 10 mm with a force range of 0–100 N applied for a period of 60 s. Optical microscopy images were acquired to identify the critical force (Fc_3) at which delamination of the layer occurred as a function of scratch distance. For each sample, three measurements were taken in different regions and the average critical force at which complete delamination of the layer occurred (Fc_3) was determined.

2.4. Corrosion resistance

The corrosion resistance of CrSiCN coatings was investigated using the potentiodynamic polarization method in distilled water and sand (10 g/L). The testing was conducted under normal temperature conditions (22 ± 1 °C) and using a magnetic stirrer. The method for evaluating the corrosion resistance involved recording the open circuit potential (E_{oc}) over 1 h and registering the potentiodynamic polarization curves between −1 V and +1.6 V (vs. Ag/AgCl), using a scan rate of 0.166 mV/s.

3. Results and discussion

3.1. Composition, morphology, and phase composition of S1–S3 steel substrates

As shown in Table 1, the EDS measurements of the used substrates revealed their significant constituents. The iron content varies among all substrates, with C45 having the highest content (86.5.± 2.9 at. %), followed by 16MnCr5 (78.1 ± 2.9 at. %), and X155CrVMo12 (57.9 ± 2.2 at. %). Similarly, the carbon content differs, with C45 exhibiting the lowest values (12.1 ± 0.4 at. %), followed by 16MnCr5 (19.2 ± 0.6 at. %), and X155CrVMo12 (28.3 ± 0.9 at. %).

Each substrate contains also different alloying elements, such as chromium, silicon, and manganese. Additionally, the Fe/C ratio provides insights into the relative proportions of iron and carbon in each substrate, with S1- X155CrVMo12 exhibiting the lowest ratio (2.0) as compared to S2 – 16MnCr5 (4.0) and S3 – C45 substrate (7.1). It can be observed that the substrates are different in terms of their Fe/C ratio, which has an impact on their mechanical, physical, and chemical properties. The differences in Fe and C content and the presence of alloying elements contribute to variations in hardness, strength, corrosion resistance, and other relevant properties. As can be seen in Fig. 1, the substrates exhibited smoother surfaces up to a roughness of ~50 nm after the polishing procedure. EDS mapping analysis was conducted in order to examine the distribution of carbon, iron (Fe), and alloying elements, and the results are depicted in Fig. 1. The EDS mapping revealed a consistent and even distribution of every element on the surface of the substrate. This

Table 1
Elemental composition (at. %) of the used substrate alloys with different Fe/C ratios.

Substrate	Fe	C	Si	Mn	Cr	Mo	V	P	S	Ni	Fe/C
X155CrVMo12	57.9 ± 2.2	28.3 ± 0.9	0.7 ± 0.02	0.3 ± 0.03	11.5 ± 0.4	0.4 ± 0.05	0.8 ± 0.05	\	\	\	2.0
16MnCr5 (1.7131)	78.1 ± 2.9	19.2 ± 0.6	0.5 ± 0.03	1.3 ± 0.06	0.9 ± 0.1		\	0.001	0.041 ± 0.001	\	4.0
C45	86.5 ± 2.9	12.1 ± 0.4	0.4 ± 0.033	1 ± 0.05	0.1 ± 0.02	\	\	0.002	0.004	0.016 ± 0.001	7.1

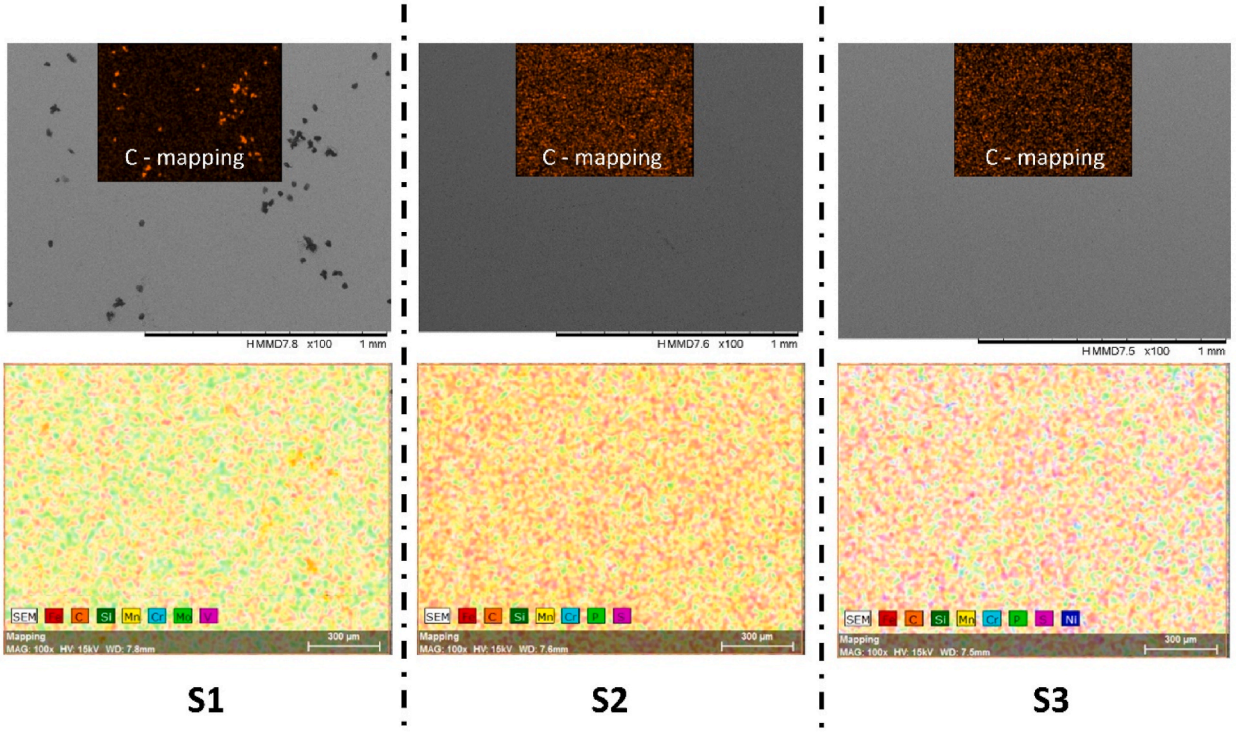

Fig. 1. SEM images and EDS elemental composition and distribution of S1–S3 substrates.

was especially noticeable in mapping the carbon (C) element, as depicted in the insets on the upper side of Fig. 1.

In the case of S1, precipitated carbide particles [37] were observed. The appearance of these carbide particles is related to the heat treatment process, especially tempering, which involves heating the quenched steel to temperatures below the recrystallization point

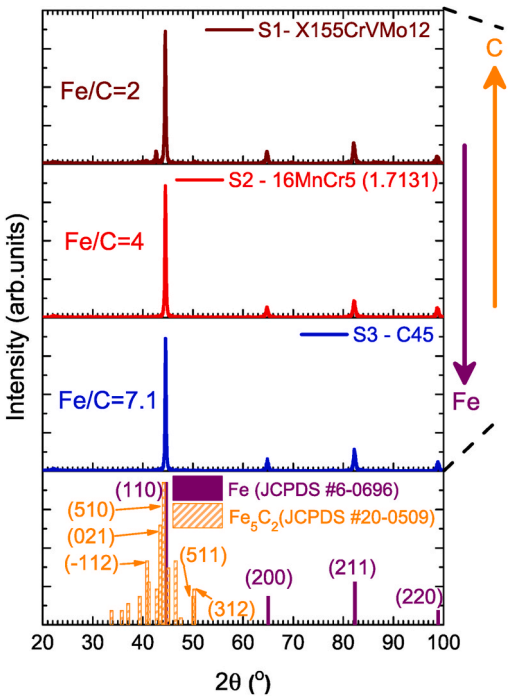

Fig. 2. XRD patterns of S1–S3 substrates with different Fe/C ratios.

and holding it at this temperature for a specific period of time, followed by controlled cooling. During tempering, chemical reactions and atomic diffusion occur within the steel, forming carbide precipitates. Also, no surface cracks or other defects were observed in the case of S2 and S3 substrates.

The XRD diffractograms (Fig. 2) corresponding to the substrates reveal patterns equivalent to different crystal structures such as Fe and Fe_5C_2. The cubic α-Fe (a = 2.8660), identified by JCPDS#6–0696, is observed in the case of all investigated substrates, indicating that iron is a common component across all substrates. On the other hand, the monoclinic iron carbide (Fe_5C_2 - JCPDS#20–0509), is observed only in the case of S1 - X155CrVMo2 substrate for peaks centered at 39.8^0, $40.6^{0,}$ and 42.6^0. The presence of monoclinic Fe_5C_2 indicates the formation of iron carbide, which could be attributed to processes such as carbon diffusion or carburization [38]. This finding is in good agreement with the morphology results obtained by SEM analysis on S1 – S3 substrates and it is also supported by carbon mapping analysis depicted in Fig. 1. After analyzing the composition, morphology, and phase composition of the S1–S3 steel substrates, significant differences were observed in their surface and structural properties. These variations should be taken into consideration in the CrSiCN coatings perspective. The properties of these substrates are expected to play a crucial role in the determination the overall performance and characteristics of the final coated product. In order to fully understand how different types of substrates affect the properties of CrSiCN coatings, the elemental composition of CrSiCN coatings will be examined. By comparing the characteristics of the substrates with the resulting properties of the coatings, a better understanding of the entire coating process and of its outcomes will be accomplished.

3.2. *Elemental and phase composition of CrSiCN coatings*

In this section, the elemental composition of the CrSiCN coatings deposited on the S1–S3 steel substrates was analyzed. The focus is on how the variations in the substrates' composition and morphology influence the final composition and properties of the CrSiCN coatings. The comparison between the elemental composition data of the coatings and the initial characteristics of the substrates, was aimed to highlight the link between substrate properties and coating behavior. The elemental composition of CrSiCN coatings obtained at different N_2/C_2H_2 flow ratios, as represented by CrSiCN C30N70, CrSiCN C50N50, and CrSiCN C70N30 coatings, plays a crucial role in the determination of the coatings' mechanical and tribological properties. These compositions are designed to achieve a balance between hardness, wear resistance, and toughness, making them suitable for various industrial applications. Fig. 3 shows the variation of constituent elements and their relative proportions within each coating. The C/N ratios also provide valuable information about the relative abundance of carbon and nitrogen within the coatings.

The relatively higher carbon content compared to nitrogen results in a C/N ratio of overstoichiometric structure (~2.05). This composition indicates a carbon-rich structure with the highest Si/N ratio, which may lead to enhanced hardness and wear resistance due to the formation of the Si_3N_4 amorphous phase. However, the lower nitrogen content (C/Ñ0.3) might compromise the coating's toughness, making it less suitable for applications requiring high mechanical stresses or impact resistance. The CrSiCN C50N50 coating provides a more balanced elemental composition, exhibiting approximately C/Ñ 1.05 (stoichiometric structure), with carbon and nitrogen in equal amounts. This composition balances carbon and nitrogen, potentially offering moderate hardness, wear resistance, and improved toughness compared to CrSiCN C70N30 or CrSiCN C30N70. The XRD patterns of CrSiCN coatings (Fig. 5) clearly show the presence of face-centered cubic Cr carbides and nitrides, identified according to JCDPS no. 4-004-4288 and JCDPS no. 4-015-0322, respectively. The peaks located at about 39°, 43° and 65° were ascribed to (111), (200) and (220) planes mentioned in the previous standards. Since no maxima associated to SiN_x phase were identified in the diffractograms, one can assume that nanocrystalline CrN and CrC particles are embedded in an amorphous matrix. In this context, several factors could explain the similarity of XRD patterns.

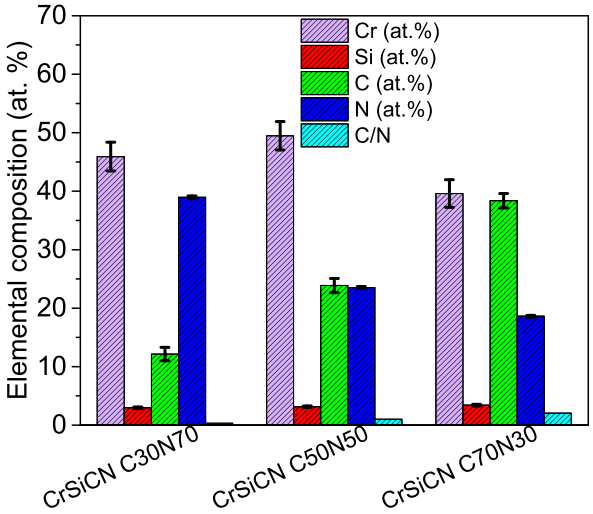

Fig. 3. Composition variation of CrSiCN coatings.

Certain crystal structures can accommodate a range of substitutions without significantly altering their lattice parameters [39]. If the chosen deposition conditions favor the formation of these stable crystal structures, they may dominate regardless of variation in C and N content. Moreover, the kinetics of the film growth could also play a significant role and support the formation of specific crystalline phases over others, outweighing the influence of elemental composition [40]. While the XRD patterns might appear identical, subtle structural changes could still exist.

The thickness of the CrSiCN coatings varied as follows: CrSiCN C30N70 had an average thickness of 1944 nm (±101 nm), CrSiCN C50N50 of 2422 nm (±140 nm), and CrSiCN C70N30 was 2446 nm (±110 nm).

3.3. Mechanical characteristics of CrSiCN coatings

3.3.1. Adhesion

The optical microscopy images of the scratch marks for the CrSiCN samples are presented in Table 2. As a general remark, characteristic scratch traces of the deposited layers on the S2 substrate showed delamination of each investigated CrSiCN coating compared to the other S1 and S3 alloys used as substrates. However, an improvement in adhesion is observed with an increase in the flow rate of C_2H_2 gas while reducing the flow rate of N_2 gas.

Fig. 5 shows the evolution of Fc_3 critical force determined for each coating as a function of the CAE gas flow rates. It can be observed that the best adhesion was recorded for the CrSiCN coatings deposited on the S1 substrate, with values ranging within 17–18 N interval. The CrSiCN C30N70 showed a strong adhesion with the S1 substrate, with an Fc_3 value of 18 N. However, on the S3 substrate, the adhesion strength decreased to 12 N, indicating that the type of the substrate can impact coating adhesion. The CrSiCN C50N50 composition had a slightly lower adhesion strength of 17 N on the S1 substrate, with a minimal reduction to 14 N on the S3 substrate, suggesting a balanced performance that ensures reliable adhesion across different materials. The CrSiCN C70N30 composition showed similar adhesion strengths as the C50N50 on the S1 substrate, with an Fc_3 of 17 N, but a decrease on the S3 substrate to 14 N, pointing to the link between coating composition and substrate interaction. Additionally, there is a general trend of increased adhesion for the coatings deposited on S2 and S3 substrates with increasing carbon content, with the highest value obtained for the CrSiCN C70N30 layer (14 N for the S3 substrate). The results were consistent for coatings deposited on S2 and S3 substrates, where a higher addition of carbon in the coating composition had a beneficial effect on adhesion. Higher carbon content in the CrSiCN composition can lead to more carbon-rich phases, such as carbonitrides and carbides [41]. These phases are assumed to strengthen the coating's matrix and enhance its adhesion to the steel substrates. Also, carbon-rich phases promote strong chemical bonds with the steel substrates, exhibiting a better interfacial adhesion as seen for CrSiCN coatings deposited on the S1 substrate (Fig. 4).

Therefore, by adjusting the C/N ratio, the distribution and size of carbonitride, amorphous carbon, and carbide phases can be tailored. A well-dispersed and homogeneous distribution of these phases helps to reduce the stress concentrations and crack initiation sites, improving the overall adhesion and resistance to delamination. It can be concluded that the obtained F_{c3} values confirm the observations on the optical microscopy images at the end of the scratch testing.

3.3.2. Hardness, friction and wear performance

Fig. 6 shows the evolution of the R_a roughness parameter determined for each sample after coating. The uncoated surfaces are also presented. It can be observed that all uncoated alloys exhibited similar roughness before deposition. For a good evaluation of the results, it is essential to have alloys with similar roughness. After the deposition of the coating, the roughness increased significantly regardless of the nature of the coating. By comparing the alloys, there are some differences, and those coated by C70N30 presented the smallest values. However, there are no significant differences in roughness in the case of the same coating deposited on different alloys, indicating that the type of alloy did not influence the roughness of coatings.

The Vickers hardness values for the substrates were determined to be 276 ± 10 HV for S1, 219 ± 6 HV for S2, and 224 ± 13 HV for

Table 2
Optical microscopy images of the scratch traces for the CrSiCN samples deposited on S1–S3 substrates.

Q C_2H_2/N_2	Substrate	CrSiCN
30/70		
50/50	S1	
70/30		
30/70		
50/50	S2	
70/30		
30/70		
50/50	S3	
70/30		

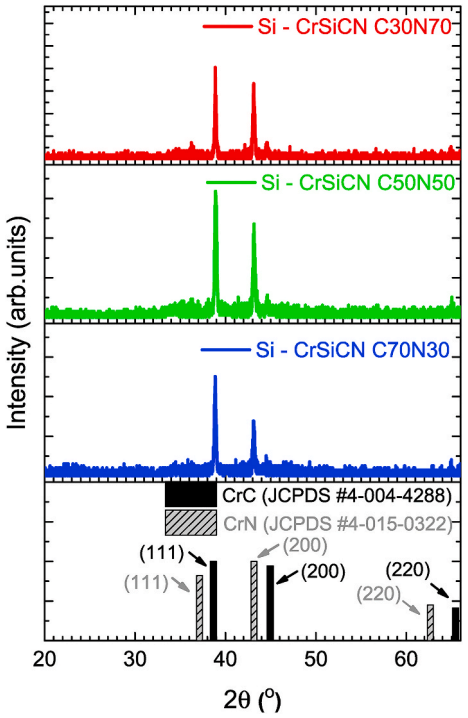

Fig. 4. Evolution of the critical force (Fc_3) for complete coating delamination.

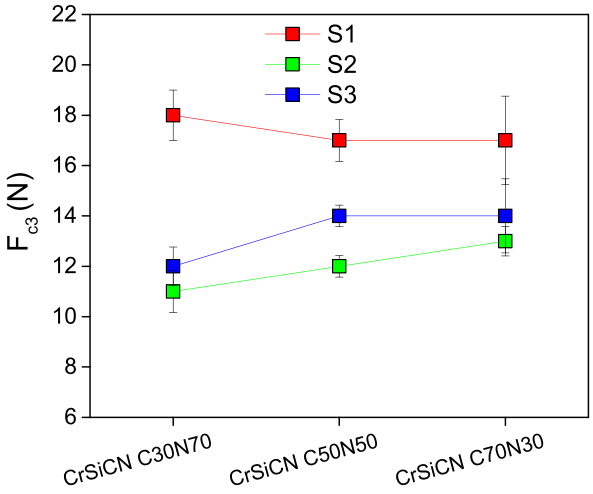

Fig. 5. XRD patterns of CrSiCN coatings.

S3, indicating a higher hardness of S1 substrate as compared to S2 and S3 substrates. The friction and wear characteristics of the CrSiCN coatings were assessed while exposing coatings to a corrosive environment containing distilled water and sand. The results of the tribological tests were quantified by deriving the variations of friction coefficient (μ) versus sliding distance and the wear rate (K).

As shown in Fig. 7, all the coatings exhibited lower friction coefficients (μ values) compared to the S1–S3 substrates. The friction coefficient of the CrSiCN C50N50 coating remained nearly constant, indicating typical behaviour observed in steady-state wear conditions [42,43]. On the other hand, the CrSiCN C70N30 coating showed an unstable friction coefficient evolution, with fluctuations during wear testing in the case of S1 and S3 substrates. The CrSiCN C50N50 coating demonstrated the best friction behaviour compared to CrSiCN C70N30 and CrSiCN C30N70, with the lowest μ values and a stable friction evolution.

As can be seen in Fig. 8, it becomes evident that the composition of the CrSiCN coating significantly influences its wear resistance. The C50N50 composition demonstrates the best wear performance in the case of each investigated substrate, making it an excellent choice for applications where wear resistance is critical. In this case, the C/N ratio proved to be an important tool for selecting the

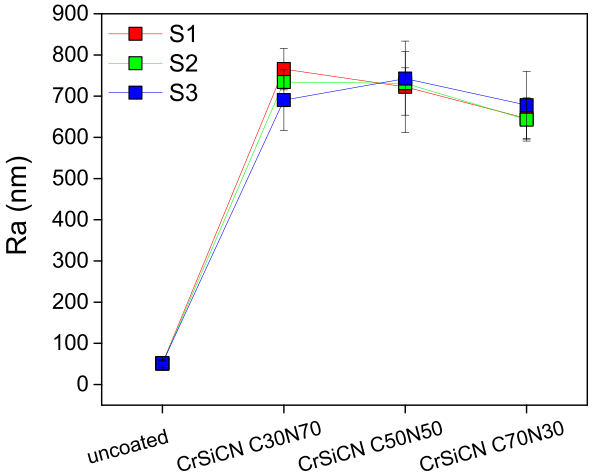

Fig. 6. Evolution of Ra roughness parameter of uncoated and coated surfaces.

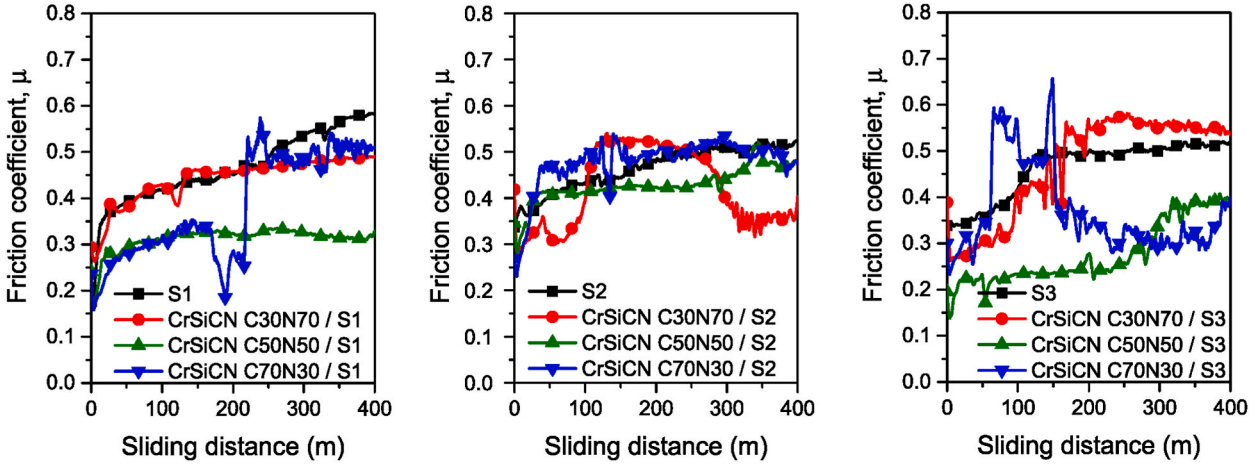

Fig. 7. Evolution of CrSiCN coatings' friction coefficient substrates as a function of sliding distance.

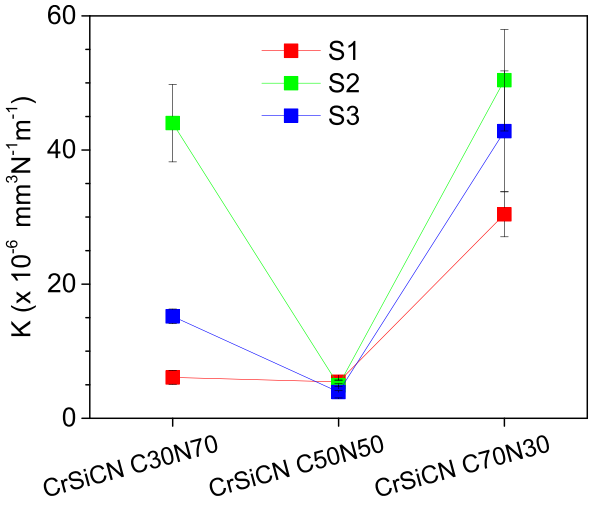

Fig. 8. Wear rate, K, for CrSiCN coatings deposited on S1–S3 substrates.

appropriate CrSiCN coating composition based on specific application requirements. Also, the C70N30 composition exhibits the highest wear rate, suggesting that it may be less suitable for applications with high wear requirements.

The results presented by SEM micrographs of the worn surfaces confirmed the previous μ and K evolutions according to each substrate (Fig. 9). As observed, the best-performing coating from both friction and wear points of view (i.e., CrSiCN C50N50) showed the mildest wear process among all the investigated coatings, regardless of the substrate, resulting underlined by the evident decrease in the wear track width. Following the analysis of the worn surface, one can note that oxidation, adhesion, and polishing are the main processes involved in the wear mechanism. A mild polishing wear, without pronounced defects, dominated the wear behaviour of CrSiCN C30N70, showing less surface damage. Additionally, when coating was applied on S3 alloy, a significant amount of wear debris underwent plastic deformation, resulting in the formation of plate-shaped wear particles with high adherence to the worn surfaces. On the contrary, a minor abrasive wear process was observed in the case of CrSiCN C50N50, pointed out by the presence of 3rd body wear scars in combination with adherent material in some surface areas of coated S3. Despite these findings, shallow marks were exhibited by the mentioned coatings, which explain the lowest wear values obtained and the smooth μ evolution. The unstable friction coefficient of CrSiCN C70N30 correlated with the highest K value in the case of S1 and S3, can be explained by the presence of wider wear tracks with accumulated debris as a consequence of the sliding surfaces being in contact. The extent of wear debris accumulated in this case is indicative of a severe wear damage and the observed general features are responsible for the high friction and the low wear resistance. In the first stage, since the contact surfaces are subjected to high pressure, the surface irregularities deform, leading to material transfer and increased contact area. Further, under continued sliding, the shear stress appears, leading to the detachment of the material and thus creating an unstable friction behaviour. Moreover, as pointed out by the EDS elemental distribution images, the wear process was also found to be dominated by an oxidative mechanism, more visible for CrSiCN C70N30 coatings. However, since no Fe traces arising from the substrate were revealed, one can exclude a severe degradation of the investigated coatings in the present conditions.

For wear resistance, the CrSiCN C30N70 revealed a wear rate of 6.08×10^{-6} $mm^3N^{-1}m^{-1}$ on the S1 substrate, but this rate significantly increased to 44×10^{-6} $mm^3N^{-1}m^{-1}$ on the S2 substrate, and then to 15.2×10^{-6} $mm^3N^{-1}m^{-1}$ on the S3 substrate,

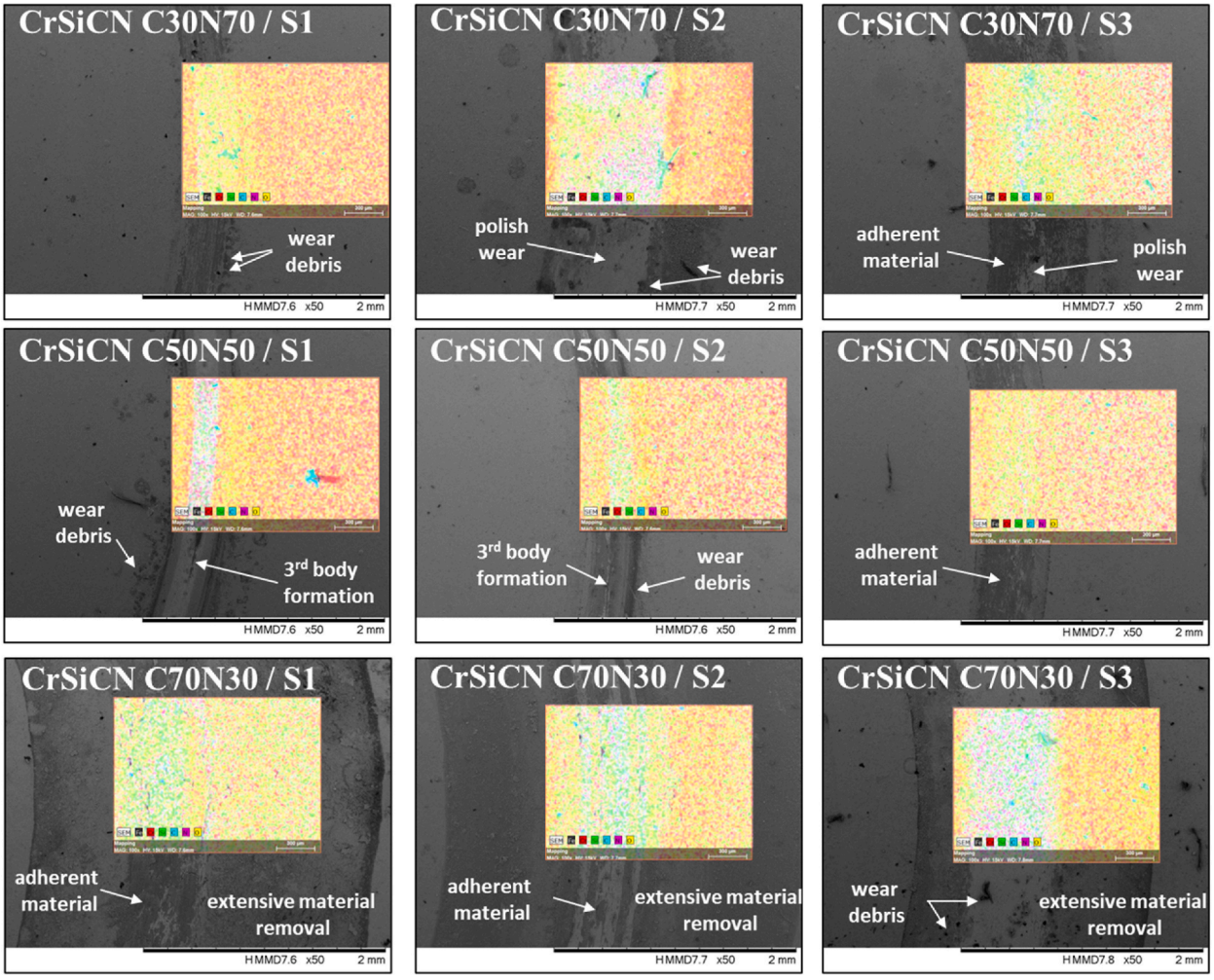

Fig. 9. SEM micrographs and EDS elemental distribution images of the worn surfaces.

indicating possible difficulties to operational conditions and substrate effects. The CrSiCN C50N50 composition emerged as particularly wear-resistant, maintaining a low wear rate of 5.42×10^{-6} $mm^3N^{-1}m^{-1}$ on the S1 substrate, further improving to 4.89×10^{-6} $mm^3N^{-1}m^{-1}$ on the S2 substrate, and demonstrating the best performance with 3.9×10^{-6} $mm^3N^{-1}m^{-1}$ on S3 substrate, indicating its durability across varied conditions. The CrSiCN C70N30 composition exhibited the highest wear rates, with 30.4×10^{-6} $mm^3N^{-1}m^{-1}$ on S1 substrate, increasing to 50.4×10^{-6} $mm^3N^{-1}m^{-1}$ on the S2 substrate, and 42.8×10^{-6} $mm^3N^{-1}m^{-1}$ on the S3 substrate, which could limit its utility in high-wear scenarios.

3.4. Corrosion resistance

Fig. 10 shows the changes in the open circuit potential (E_{oc}) over time (a, b, c) and the corresponding potentiodynamic curves (d, e, f) for substrates (S1, S2, S3) coated with CrSiCN coatings. The coated specimens exhibited an increasing tendency towards more electropositive values as compared with the investigated S1–S3 substrates. The fluctuations observed may be attributed to the instability of the oxide layer formed on its surface, as a result of surface passivation. The evolution of E_{oc} for the S1 substrate demonstrated a consistent and stable behaviour during the corrosion test, suggesting the coating's effectiveness in providing corrosion protection. However, fluctuations were observed in the E_{oc} values for S2 and S3 substrates, particularly noticeable for the layers deposited with different C_2H_2 and N_2 flow rates.

To further investigate the effect of carbon and nitrogen content on corrosion behaviour, corrosion parameters such as polarization resistance (R_p) were determined and they are presented in Table 3. The results indicate increased carbon content resulted in higher R_p values for the coatings deposited on S1 and S3 substrates. This suggests that higher carbon content enhances the protective properties of the CrSiCN coating on these substrates. However, for the S2 substrate, the coating with the highest polarization resistance (R_p) was the one deposited with a C_2H_2 flow rate of 30 sccm and an N_2 flow rate of 70 sccm, indicating that this specific composition offered superior corrosion protection for this particular substrate.

The most electropositive value of corrosion potential was demonstrated by the CrSiCN coating deposited on the S1 substrate, indicating relatively better corrosion resistance compared to the S2 or S3 substrates. Among all substrates, the CrSiCN C50N70 coating on the S1 substrate exhibited the highest corrosion potential (E_{corr}) with a value of 54.629 mV, indicating the best corrosion resistance among the three coatings with the same composition. However, all coatings exhibited an E_{corr} more electropositive than all uncoated substrates, indicating an increase in corrosion resistance of steels by coating them. Nevertheless, based on the E_{corr} values, it can be stated that the CrSiCN C50N70 coating has the best corrosion resistance.

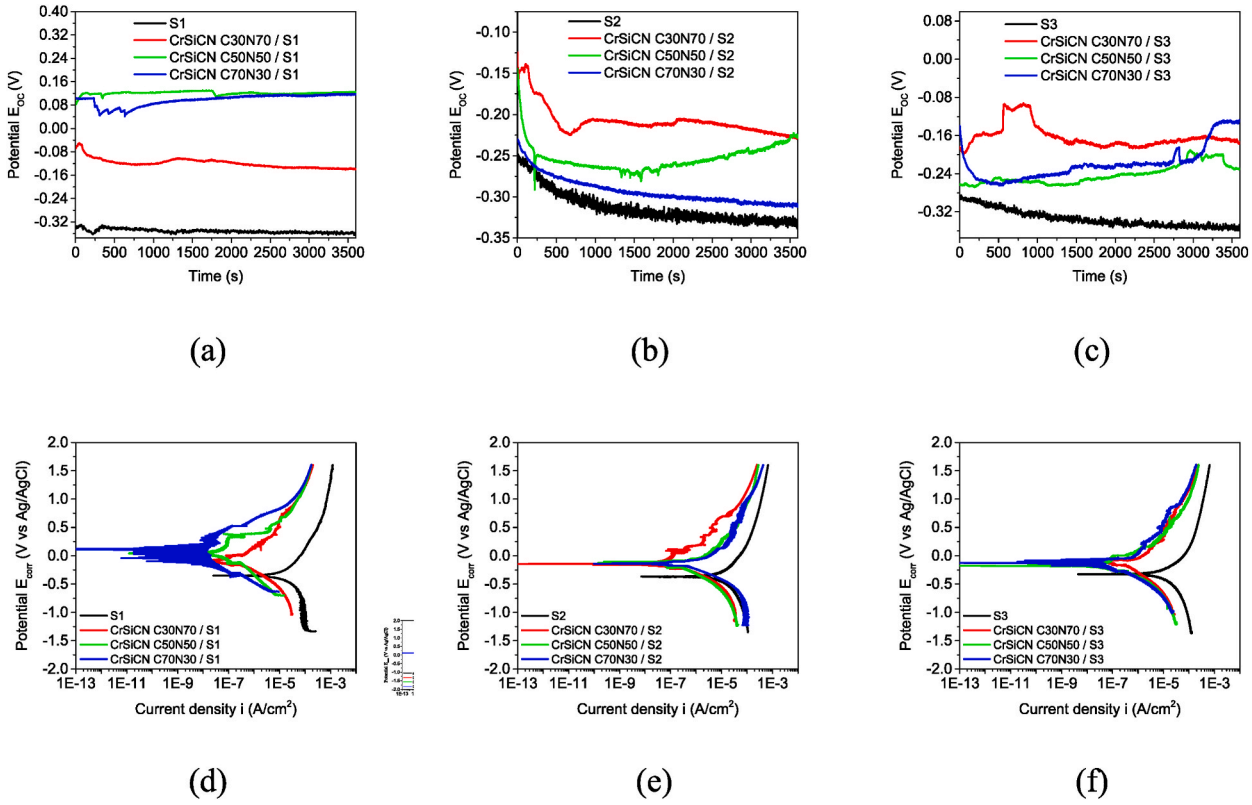

Fig. 10. Evolution of open circuit potential over time (a,b,c) and potentiodynamic curves (d,e,f) for steel substrates (S1, S2, S3) coated with CrSiCN thin films.

Table 3
Corrosion parameters derived from Tafel plots for CrSiCN coatings deposited on S1–S3 substrates (E_{corr}: corrosion potential; i_{corr}: corrosion current density; R_p: polarization resistance).

Coating	Substrate	E_{oc} (mV)	E_{corr} (mV)	i_{corr} (μA/cm^2)	R_p (Ω*10^{-3})	Pe (%)
–	S1	−363.14	−360.577	5.275	8	–
CrSiCN C30N70	S1	−138.63	−125.376	0.089	666	98.31
CrSiCN C50N50		124.83	54.629	0.021	3603	99.60
CrSiCN C70N30		116.86	28.024	0.008	12728	99.85
–	S2	−333.39	−338.39	4.638	14	–
CrSiCN C30N70	S2	−227.88	−146.66	0.064	998	98.62
CrSiCN C50N50		−226.96	−118.432	0.034	484	99.27
CrSiCN C70N30		−311.61	−139.013	0.020	402	99.57
–	S3	−350.57	−357.968	13.045	11	–
CrSiCN C30N70	S3	−174.21	−113.312	0.077	300	99.41
CrSiCN C50N50		−230.03	−167.774	0.113	945	99.13
CrSiCN C70N30		−127.59	−118.113	0.109	1996	99.16

The corrosion current density (i_{corr}) was the lowest for the CrSiCN C70N30 coating on the S1 substrate (0.008 μA) and it had the highest polarization resistance of 12.728 Ω, which implied that it had the slightest tendency to corrode. Moreover, the corrosion current density (i_{corr}) was also found to be the lowest for the CrSiCN C50N50 coating on the S1 substrate (0.021 μA/cm^2) as well as CrSiCN C70N30 coating on the S2 substrate (0.020 μA/cm^2), indicating the best corrosion resistance among all the others investigated coatings.

Considering the coatings' protective efficiency (Pe), calculated according Eq. (2) and presented in Table 3, one can note that, regardless of their composition and the substrate type, high values were presented by all the coated specimens (Pe ~ 98–99 %). Only minor differences, as a function of C/N ratio, were observed, as follows: i) the highest calculated value was proved by CrSiCN C70N30_S1 (Pe = 99. 85 %); ii) a higher carbon content led to higher coating protection when S1 and S2 were used as substrates; iii) on the other hand on S3 substrate, it was found the highest Pe value for CrSiCN C30N70, in correlation with the corrosion density value associated.

$$Pe = \left(1 - \frac{icorr\_coating}{icorr\_substrate}\right) \quad (2)$$

3.5. Resistance to real exploitation

Based on the adhesion tests and corrosion resistance, both CrSiCN C70N30 and CrSiCN C50N50 proved to have the highest resistance at the corrosive attack of distilled water solution with sand. However, there are minor differences between these two coatings. Based on the tribological performance performed in the laboratory, the lowest friction coefficient was found for CrSiCN C50N50 (S1) and CrSiCN C70N30 (S3). In contrast, the lowest wear rate was determined for CrSiCN C50N50, whatever the substrates were.

It was challenging to decide which coating is performed the best, however CrSiCN C50N50 can be a promising solution for testing in real long service life. Thus, this coating was selected to be used as a coating for a tool used to process the wood (Fig. 11). Some types of wood used for testing are presented in Fig. 12, as well as different hard or soft timber (spruce, beech, ash). The wood was sometimes used with adhesive (such as urelite and resin). These processes attempted to simulate the real conditions of working tools in a wood factory. Table 4 shows the results obtained for the coated tool compared with the uncoated tool.

One may see that the improved time depends on the type and thickness of wood as wells as on the type of planing (aggressive or easy). For example, the uncoated tools cut of 671.3 linear meters of beech (50 mm thickness). By coating the tools edges, 1212.7 linear meters were cut, meaning an increase of 44.6 %.

In Fig. 11, the degradation area can be found on coated prototypes. The distribution of these deteriorated areas is irregular and varies in size. These can be either material removed and reattached during the cutting process, or material from the coating removed by wear process. Unfortunately, it cannot be concluded whether there is still a coating layer on the surface of the prototypes. To draw these conclusions, SEM and EDS analyses need to be performed on their surface, which cannot be done due to the large size of the samples exceeding the size of analysis chamber of an SEM system. If it was to attempt cutting small pieces from the prototypes, the areas of interest would be damaged during cutting. In conclusion, based on these tests, only the service-life of the coated parts compared to the uncoated ones can be determined, envisaged in linear meters cut with coated and uncoated samples.

4. Discussions

The present work investigated CrSiCN coatings deposited by cathodic arc evaporation on different steel substrates as a possible coating to cover the wood-cutting tools. The effect of the C/N ratio on coatings' structural, mechanical, tribological, and corrosion resistance was also studied. The experimental outcomes have demonstrated that the ratio between N_2 and C_2H_2 is one of the key deposition conditions that can control the properties of the CrSiCN coatings. It is shown that the C50N50 films are superior to C70N30 or C30N70 films in terms of morphology, hardness, corrosion, and friction behaviour. Thus, CrSiCN C50N50 was selected to coat tools

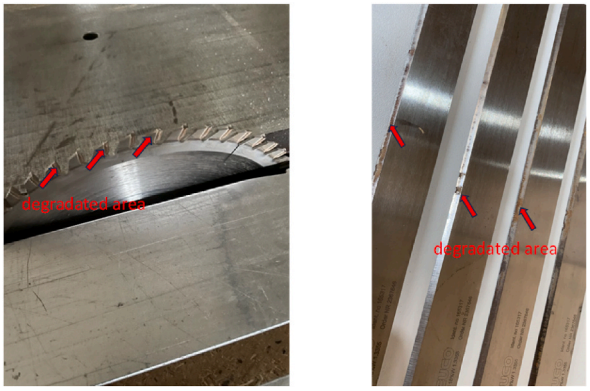

Fig. 11. Coated tools after tests: (a) for cutting; (b) for planning. Red arrows are attributed to degradation area.

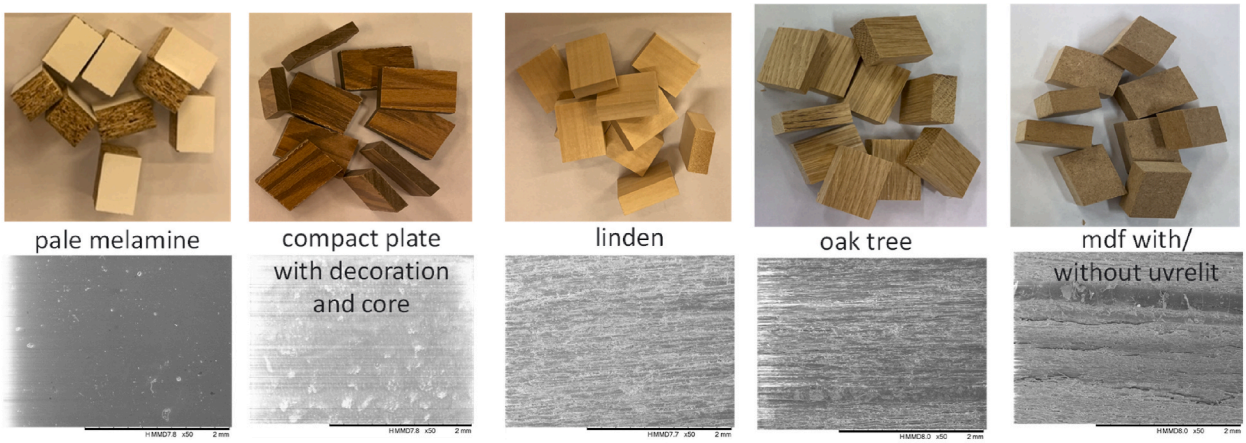

Fig. 12. Image of the wood used for testing the wood tool coated by CrSiCN coatings.

Table 4
Results of service life of a coated tool in comparison with an uncoated tool (aggressive planing = 5 mm/one pass; easy planing = 2.5 mm/one pass).

Type of wood	Type of process	Quantity Uncoated tools	Quantity Coated tools
Laminated MDF (3 layers of MDF with adhesive)	cut	1798.5 linear meters	3997.5 linear meters
MDF + adhesive + Beech	cut	2324.2 linear meters	4920.8 linear meters
MDF without adhesive (18 mm thickness)	cut	4846.9 linear meters	13681.1 linear meters
MDF without adhesive (12 mm thickness)	cut	2281.6 linear meters	6403.4 linear meters
Beech (50 mm thickness)	cut	671.3 linear meters	1212.7 linear meters
Beech (26 mm thickness)	cut	2402.7 linear meters	4767.3 linear meters
Pal melamine (18 mm thickness)	cut	1830.4 linear meters	4538.6 linear meters
Sprunce (50 mm thickness)	aggressive planing	77.4 m^2	122.6 m^2
Pine (26 thickness)	easy planing	68.1 m^2	136.9 m^2
Ash (26 mm thickness)	easy planing	22.0 m^2	50.8 m^2
Ash (50 mm thickness)	aggressive planing	5.2 m^2	8.0 m^2
Beech (50 mm thickness)	aggressive planing	178.1 m^2	276.3 m^2

for working in real service life. The wood machining tests showed that the coated tools are more resistant than the uncoated ones. During the process, the coated tools exhibited greater resistance than the uncoated ones, indicating a beneficial effect of the coatings. This research showed that the CrSiCN C50N50 coatings could be a solution for improving the cutting tools' service life, which can lead to a high productivity machining of wood and wood-based products and a reduction of power consumption, surface finish, and production rates. Moreover, this surface improvement is an advantage for enhancing productivity and reducing the operating cost.

In wood machining, corrosion and wear are two complex processes influenced by adhesion and hardness properties. Regularly, the cutter surfaces need to have a high hardness across a wide temperature range. In the context of coated surfaces, it is crucial for the coating to demonstrate satisfactory adhesion properties. For example, when the tools cut the oak wood, the coated cutter surfaces should act as a wear-resistant barrier and protection from corrosive environments. During a wood machining, the coating can be detached by abrasion or peeling off due to poor adhesion between the coating and steel as well as due to the brittleness of the coating. Furthermore, the high working temperatures can be the main reason for the coating delamination.

For example, the machining process of oak wood is the harshest cutting operation in which the cutter endures repeated cycles of cutting and idling. During the cutting, a significant amount of heat is released while idling. However, the wood is a pure heat conductor, so the heat transfer to the workpiece is bordering, released into the air, or collected in the cutter holder. Therefore, the cutting edge endures many cyclic fluctuations in temperature. Based on this statement, the coatings should also be resistant to high temperatures, wear, and corrosion. Thus, the field of wood-cutting tools still needs further research. It appears that forthcoming research should focus on choosing one method for coating preparation on a clearly defined substrate. The choice of the best coatings is much more complex because these should have high hardness, good adhesion to the substrate, stability at high temperatures, relatively low friction coefficient and wear rate, and a good corrosion resistance. The service life tests of coated tools should be limited to one specific wood species and the same testing parameters. Also, it is essential to compare the research results with the uncoated tools.

5. Conclusions

The study aimed to enhance the mechanical and anticorrosion properties of CrSiCN coatings and to identify the optimal deposition parameters for coatings with superior mechanical and anticorrosive properties. The results showed that the C/N ratio was critical, the coatings with higher carbon content presented slightly enhanced corrosion resistance, being able to withstand similar real-life operating conditions. The optimal deposition parameters for superior corrosion protection depended on the specific substrate. CrSiCN coatings exhibited high hardness, wear resistance, and low friction coefficient, making them promising for industrial woodworking applications.

Overall, the results indicate that the CrSiCN C30N70 coating on the S1 substrate consistently exhibited the best corrosion resistance among the investigated samples. Additionally, the performance of the CrSiCN coatings was influenced by the carbon and nitrogen content, with different substrates showing variations in corrosion behaviour.

The findings provided valuable insights into the properties of CrSiCN coatings and their potential applications in the woodworking industry.

Funding

This research was funded by a grant of the Romanian National Authority for Scientific Research and Innovation, CCCDI – UEFISCDI, project number COFUND-*M*-ERANET-3-HardCoat-1, no. 311/2022 (INOE2000) and no. 312/2022 (Drugon International SRL), Romania, within PNCDI III.

CRediT authorship contribution statement

Iulian Pana: Writing – review & editing, Writing – original draft, Methodology. **Anca Constantina Parau:** Methodology, Investigation. **Mihaela Dinu:** Methodology, Investigation. **Catalin Vitelaru:** Writing – review & editing, Methodology, Investigation. **Diana Maria Vranceanu:** Writing – review & editing, Validation, Project administration, Methodology, Investigation. **Thomas Lindner:** Writing – review & editing, Methodology, Conceptualization. **Alina Vladescu (Dragomir):** Writing – review & editing, Supervision, Project administration, Methodology, Investigation, Conceptualization.

Declaration of competing interest

The authors declare that they have no known competing financial interests or personal relationships that could have appeared to influence the work reported in this paper.

Acknowledgements

The work was supported by the Core Program within the National Research Development and Innovation Plan 2022–2027, carried out with the support of MCID, project no. PN 23 05 (id: PN11N-03-01-2023) and through Program 1—Development of the national research-development system, Subprogram 1.2—Institutional performance-Projects to finance the excellent RDI, Contract no. 18PFE/December 30, 2021.

A.V.D. thanks to Tomsk Polytechnic University within the framework of the Tomsk Polytechnic University-Competitiveness Enhancement Program. A.V.D, A.C.P. M.D., I.P, C.V. acknowledge the support from the National Research Development and Innovation Plan 2022–2027, Core Program, Project no: PN 23 05, contract no PN11N-03-01-2023, and through Program 1- Development of the National Research-Development system, Sub-program 1.2 - Institutional Performance - Projects to Finance the Excellent RDI, Contract no. 18PFE/December 30, 2021.

References

[1] S. Cordier, F. Robichaud, P. Blanchet, B. Amor, Regional environmental life cycle consequences of material substitutions: the case of increasing wood structures for non-residential buildings, J. Clean. Prod. 328 (2021), https://doi.org/10.1016/j.jclepro.2021.129671.

[2] R. Ojurović, M. Moro, K. Šegotić, T. Grladinović, L. Oblak, Analysis of the investment in wood processing and furniture manufacturing entities by key factors of competitiveness, Drv. Ind. 64 (2013), https://doi.org/10.5552/drind.2013.1235.

[3] H. Thomson, C. Liddell, The suitability of wood pellet heating for domestic households: a review of literature, Renew. Sustain. Energy Rev. 42 (2015), https://doi.org/10.1016/j.rser.2014.11.009.

[4] A. Keskisaari, T. Kärki, Utilization of industrial wastes from mining and packaging industries in wood-plastic composites, J. Polym. Environ. 26 (2018), https://doi.org/10.1007/s10924-017-1052-z.

[5] R. Salim, J. Johansson, Automation decisions in investment projects: a study in the Swedish wood products industry, in: Procedia Manuf, 2018, https://doi.org/10.1016/j.promfg.2018.06.081.

[6] M. Schubert, G. Panzarasa, I. Burgert, Sustainability in wood products: a new perspective for handling natural diversity, Chem. Rev. 123 (2023), https://doi.org/10.1021/acs.chemrev.2c00360.

[7] E. Medvedovski, Wear-resistant engineering ceramics, Wear 249 (2001), https://doi.org/10.1016/S0043-1648(01)00820-1.

[8] Y. Wang, B. Ou, P. Zhu, B. Niu, Y. Guo, Q. Zhi, High mechanical strength aluminum foam epoxy resin composite material with superhydrophobic, anticorrosive and wear-resistant surface, Surface. Interfac. 29 (2022), https://doi.org/10.1016/j.surfin.2022.101747.

[9] R. Qiu, Z. Li, Z. Wu, Enhanced anti-icing and anti-corrosion properties of wear-resistant superhydrophobic surfaces based on Al alloys, Mater. Res. Express 6 (2019), https://doi.org/10.1088/2053-1591/aafdf1.

[10] T. Tokunaga, M. Ohno, K. Matsuura, Coatings on Mg alloys and their mechanical properties: a review, J. Mater. Sci. Technol. 34 (2018), https://doi.org/10.1016/j.jmst.2017.12.004.

[11] C.M. Cotrut, A.C. Parau, A.I. Gherghilescu, I. Titorencu, I. Pana, D.V. Cojocaru, V. Pruna, L. Constantin, I. Dan, D.M. Vranceanu, A. Vladescu, Mechanical, in vitro corrosion resistance and biological compatibility of cast and annealed Ti25Nb10Zr alloy, Metals 7 (2017), https://doi.org/10.3390/met7030086.

[12] F. Klocke, T. Krieg, Coated tools for metal cutting - features and applications, CIRP Ann. - Manuf. Technol. 48 (1999), https://doi.org/10.1016/S0007-8506(07)63231-4.

[13] P.R. Chalker, S.J. Bull, D.S. Rickerby, A review of the methods for the evaluation of coating-substrate adhesion, Mater. Sci. Eng. A. 140 (1991), https://doi.org/10.1016/0921-5093(91)90482-3.

[14] B. Bakhit, A. Akbari, F. Nasirpouri, M.G. Hosseini, Corrosion resistance of Ni-Co alloy and Ni-Co/SiC nanocomposite coatings electrodeposited by sediment codeposition technique, Appl. Surf. Sci. 307 (2014), https://doi.org/10.1016/j.apsusc.2014.04.037.

[15] Y. Gu, K. Xia, D. Wu, J. Mou, S. Zheng, Technical characteristics and wear-resistant mechanism of nano coatings: a review, Coatings 10 (2020), https://doi.org/10.3390/coatings10030233.

[16] B. Prakash, J. Hardell (Eds.), Coatings Tribology (2021), https://doi.org/10.3390/books978-3-03943-694-1.

[17] C. Nouveau, M.A. Djouadi, C. Decès-Petit, P. Beer, M. Lambertin, Influence of CrxNy coatings deposited by magnetron sputtering on tool service life in wood processing, Surf. Coatings Technol. (2001) 142–144, https://doi.org/10.1016/S0257-8972(01)01092-1.

[18] Y. Qiu, S. Zhang, B. Li, Y. Wang, J.W. Lee, F. Li, D. Zhao, Improvement of tribological performance of CrN coating via multilayering with VN, Surf. Coatings Technol. 231 (2013), https://doi.org/10.1016/j.surfcoat.2012.03.010.

[19] M. Durmaz, B. Kilinc, E. Abakay, U. Sen, S. Sen, Tribological properties of CrN coatings deposited by nitro-chromizing treatment on AISI D2 steel, in: AIP Conf. Proc., 2015, https://doi.org/10.1063/1.4914225.

[20] G. Aktaş Çelik, Ş.H. Atapek, Ş. Polat, A. Obrosov, S. Weiß, Nitriding effect on the tribological performance of CrN-, AlTiN-, and CrN/AlTiN-coated DIN 1.2367 hot work tool steel, Materials 16 (2023), https://doi.org/10.3390/ma16072804.

[21] J.Z. Kong, C. Li, X.Y. Sun, Y. Xuan, H.F. Zhai, A.D. Li, Q.Z. Wang, F. Zhou, Improved tribological properties and corrosion protection of CrN coating by ultrathin composite oxide interlayer, Appl. Surf. Sci. 541 (2021), https://doi.org/10.1016/j.apsusc.2020.148606.

[22] L. Aissani, C. Nouveau, M.J. Walock, H. Djebaili, A. Djelloul, Influence of vanadium on structure, mechanical and tribological properties of CrN coatings, Surf. Eng. 31 (2015), https://doi.org/10.1179/1743294415Y.0000000043.

[23] F. Cai, X. Huang, Q. Yang, Mechanical properties, sliding wear and solid particle erosion behaviors of plasma enhanced magnetron sputtering CrSiCN coating systems, Wear (2015) 324–325, https://doi.org/10.1016/j.wear.2014.11.008.

[24] E. Lugscheider, O. Knotek, C. Barimani, S. Guerreiro, H.K. Zimmermann, Cr-C-N coatings deposited with different reactive carbon carrier gases in the arc PVD process, Surf. Coatings Technol. (1997) 94–95, https://doi.org/10.1016/S0257-8972(97)00448-9.

[25] P. Panjan, M. Čekada, R. Kirn, M. Soković, Improvement of die-casting tools with duplex treatment, Surf. Coatings Technol. (2004) 180–181, https://doi.org/10.1016/j.surfcoat.2003.10.119.

[26] A. Gilewicz, B. Warcholinski, P. Myslinski, W. Szymanski, Anti-wear multilayer coatings based on chromium nitride for wood machining tools, Wear 270 (2010), https://doi.org/10.1016/j.wear.2010.09.002.

[27] F. Schuster, F. Maury, J.F. Nowak, C. Bernard, Characterization of chromium nitride and carbonitride coatings deposited at low temperature by organometallic chemical vapour deposition, Surf. Coatings Technol. 46 (1991), https://doi.org/10.1016/0257-8972(91)90170-2.

[28] J.H. Jeon, C.S. Jang, S.Y. Yoon, B.C. Shin, K.H. Kim, Effects of Si addition on the characteristic evolution and syntheses of nanocomposite Cr-Si-C-N coatings prepared by a hybrid coating system, Surf. Coatings Technol. 200 (2005), https://doi.org/10.1016/j.surfcoat.2005.08.042.

[29] Y.L. Su, S.M. Chiu, W.H. Kao, H.C. Hsueh, T.Y. Hsieh, Mechanical, tribological, and corrosive properties of NbCrCx and NbCrCxNy coatings with various nitrogen and carbon contents, Metals 13 (2023), https://doi.org/10.3390/met13081488.

[30] M. Hatakeyama, T. Tsuchiya, S.W. Lee, K. Matsuda, Y. Aoi, M. Nose, Influence of iron diffusion on the oxidation resistance of CrSiCN hard coatings, Mater. Trans. 63 (2022), https://doi.org/10.2320/matertrans.MT-MA2022014.

[31] Y. Fu, F. Zhou, Q. Wang, M. Zhang, Z. Zhou, Electrochemical and tribocorrosion performances of CrMoSiCN coating on Ti-6Al-4V titanium alloy in artificial seawater, Corros. Sci. 165 (2020), https://doi.org/10.1016/j.corsci.2019.108385.

[32] Q. Wang, Z. Wu, F. Zhou, J. Yan, Comparison of crack resistance between ternary CrSiC and quaternary CrSiCN coatings via nanoindentation, Mater. Sci. Eng. A. 642 (2015), https://doi.org/10.1016/j.msea.2015.07.024.

[33] J. Du, H. Zhou, C. Sun, H. Kou, Z. Ma, X. Wang, J. Dai, Growth structure effect on the corrosion resistance and mechanical properties of crNx COATING, Surf. Rev. Lett. 27 (2020), https://doi.org/10.1142/S0218625X19500914.

[34] L.R. Constantin, M. Balaceanu, M. Cojocaru, M. Tărcolea, M. Dinu, COMPARATIVE INVESTIGATION OF CrN, CrCN AND CrSiCN COATINGS PREPARED BY MAGNETRON SPUTTERING, Univ. Politeh. BUCHAREST Sci. Bull. Ser. B-CHEMISTRY Mater. Sci. 78 (2016) 237–246.

[35] Z. Wu, F. Zhou, K. Chen, Q. Wang, Z. Zhou, J. Yan, L. Kwok-Yan Li, Friction and wear properties of CrSiCN coatings with low carbon content as sliding against SiC and steel balls in water, Tribol. Int. 94 (2016), https://doi.org/10.1016/j.triboint.2015.08.032.

[36] F. Cai, X. Huang, Q. Yang, R. Wei, D. Nagy, Microstructure and tribological properties of CrN and CrSiCN coatings, Surf. Coatings Technol. 205 (2010), https://doi.org/10.1016/j.surfcoat.2010.06.033.

[37] B. Markoli, S. Spaić, Effect of tempering on the microstructure and hardness of ledeburitic chromium steel X155CrVMo12.1, Int. J. Mater. Res. 98 (2007), https://doi.org/10.3139/146.101439.

[38] T. Turpin, J. Dulcy, M. Gantois, Carbon diffusion and phase transformations during gas carburizing of high-alloyed stainless steels: experimental study and theoretical modeling, Metall. Mater. Trans. A Phys. Metall. Mater. Sci. 36 (2005), https://doi.org/10.1007/s11661-005-0271-4.

[39] Materials Science of Thin Films (2002), https://doi.org/10.1016/b978-0-12-524975-1.x5000-9.

[40] I. Petrov, P.B.B. Barna, L. Hultman, J.E.E. Greene, Microstructural evolution during film growth, J. Vac. Sci. Technol. A Vacuum, Surfaces, Film. 21 (2003) S117, https://doi.org/10.1116/1.1601610.

[41] L.R. Constantin, A.C. Parau, M. Balaceanu, M. Dinu, A. Vladescu, Corrosion and tribological behaviour in a 3.5% NaCl solution of vacuum arc deposited ZrCN and Zr–Cr–Si–C–N coatings, Proc. Inst. Mech. Eng. Part J J. Eng. Tribol. 233 (2019) 158–169, https://doi.org/10.1177/1350650118774132.
[42] N.E. Beliardouh, K. Bouzid, C. Nouveau, B. Tlili, M.J. Walock, Tribological and electrochemical performances of Cr/CrN and Cr/CrN/CrAlN multilayer coatings deposited by RF magnetron sputtering, Tribol. Int. 82 (2015), https://doi.org/10.1016/j.triboint.2014.03.018.
[43] W. Zhai, L. Bai, R. Zhou, X. Fan, G. Kang, Y. Liu, K. Zhou, Recent progress on wear-resistant materials: designs, properties, and applications, Adv. Sci. 8 (2021), https://doi.org/10.1002/advs.202003739.